Abstract

Measurement of total hadronic differential cross sections in the LArIAT experiment

Elena Gramellini

2018

Abstract goes here. Limit 750 words.

Measurement of total hadronic differential cross sections in the LArIAT experiment

A Dissertation
Presented to the Faculty of the Graduate School
of
Yale University
in Candidacy for the Degree of
Doctor of Philosophy

by
Elena Gramellini

Dissertation Director: Bonnie T. Fleming

Date you'll receive your degree

A mia mamma e mio babbo,

grazie per le radici e grazie per le ali.

To my mom and dad,

thank you for the roots and thank you for the wings.

Contents

Acknowledgements

"*Dunque io ringrazio tutti quanti.*
Specie la mia mamma che mi ha fatto cosí funky."
– Articolo 31, Tanqi Funky, 1996 –

"*At last, I thank everyone.*
Especially my mom who made me so funky."
– Articolo 31, Tanqi Funky, 1996 –

A lot of people are awesome, especially you, since you probably agreed to read this when it was a draft.

Chapter 0

Total Hadronic Cross Section Measurement Methodology

This chapter describes the general procedure employed to measure a total hadronic differential cross section in LArIAT. Albeit with small differences, both the (π^-,Ar) and (K^+,Ar) total hadronic cross section measurements rely on the same procedure described in details in the following sections. We start by selecting the particle of interest using a combination of beamline detectors and TPC information (Section **??**). We then perform a handshake between the beamline information and the TPC tracking to assure the selection of the right TPC track (Section 0.2). Finally, we apply the "thin slice" method and measure the "raw" hadronic cross section (Section 0.3). A series of corrections are then evaluated to obtain the "true" cross section (Section 0.3.3).

At the end of this chapter, we show a sanity check of the methodology against MC truth information (Section 0.4).

0.1 Event Selection

The measurement of the (π^-,Ar) and (K^+,Ar) total hadronic cross section in LArIAT starts by selecting the pool of pion or kaon candidates and measuring their momentum. This is done through the series of selections on beamline and TPC information described in the next sections. The summary of the event selection in data is reported in Table 1.

0.1.1 Selection of Beamline Events

As shown in equation 5, we leverage the beamline particle identification and momentum measurement before entering the TPC as in input to evaluate the kinetic energy for the hadrons used in the cross sections measurements. Thus, we select the LArIAT data to keep only events whose wire chamber and time of flight information is registered (line 2 in in Table 1). Additionally, we perform a check of the plausibility of the trajectory inside the beamline detectors: given the position of the hits in the four wire chambers, we make sure the particle's trajectory does not cross any impenetrable material such as the collimator and the magnets steel (line 3 in in Table 1).

	Run-II Negative Polarity	Run-II Positive Polarity
Events Reconstructed in Beamline	158396	260810
Events with Plausible Trajectory	147468	240954
Beamline $\pi^-/\mu^-/e^-$ Candidate	138481	N.A.
Beamline K^+ Candidate	N.A	2837
Events Surviving Pile Up Filter	108929	2389
Events with WC2TPC Match	41757	1081
Events Surviving Shower Filter	40841	N.A.
Available Events For Cross Section	40841	1081

Table 1: Number of data events for Run-II Negative and Positive polarity

0.1.2 Particle Identification in the Beamline

In data, the main tool to establish the identity of the hadron of interest is the LArIAT tertiary beamline, in its function of mass spectrometer. We combine the measurement of the time of flight, TOF, and the beamline momentum, p_{Beam}, to reconstruct the invariant mass of the particles in the beamline, m_{Beam}, as follows

$$m_{Beam} = \frac{p_{Beam}}{c}\sqrt{\left(\frac{TOF * c}{l}\right)^2 - 1}, \tag{1}$$

where c is the speed of light and l is the length of the particle's trajectory between the time of flight paddels.

Figure 1 shows the mass distribution for the Run II negative polarity runs on the left and positive polarity runs on the right. We perform the classification of events into the different samples as follows:

- $\underline{\pi/\mu/e}$: mass $<$ 350 MeV
- <u>kaon:</u> 350 MeV $<$ mass $<$ 650 MeV
- <u>proton:</u> 650 MeV $<$ mass $<$ 3000 MeV.

Lines 4 and 5 in in Table 1 show the number of negative $\pi/\mu/e$ and positive K candidates which pass the mass selection for LArIAT Run-II data.

0.1.3 TPC Selection: Halo Mitigation

The secondary beam impinging on LArIAT secondary target produces a plethora of particles which propagates downstream. The presence of upstream and downstream collimators greatly abates the number of particles tracing down the LArIAT tertiary beamline. However, it is possible that more than one particle sneaks into the LArTPC during its readout time: the TPC readout is triggered by the particle firing the

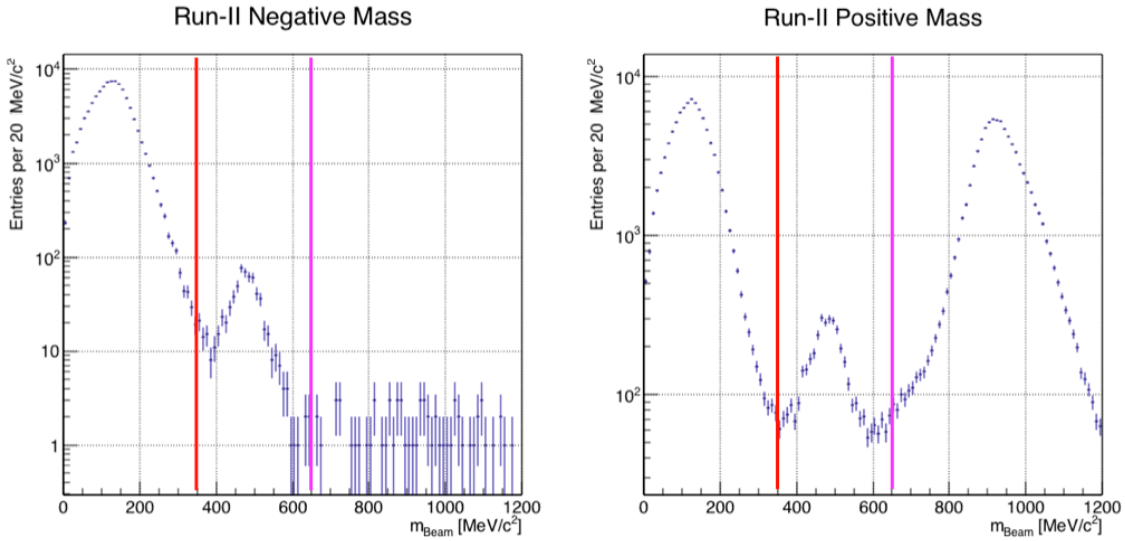

Figure 1: Distribution of the beamline mass as calculated according to equation 1 for the Run-II events reconstructed in the beamline, negative polarity runs on the left and positive polarity runs on the right. The classification of the events into $\pi^{\pm}/\mu^{\pm}/e^{\pm}$, $K^{\pm}$, or (anti)proton is based on these distributions, whose selection cut are represented by the vertical colored lines.

beamline detectors, but particles from the beam halo might be present in the TPC at the same time. We call "pile up" the additional traces in the TPC. We adjusted the primary beam intensity between LArIAT Run I and Run II to reduce the presence of events with high pile up particles in the data sample. For the cross section analyses, we remove events with more than 4 tracks in the first 14 cm upstream portion of the TPC from the sample (line 6 in in Table 1).

0.1.4 TPC Selection: Shower Removal

In the case of the (π^-,Ar) cross section, the resolution of beamline mass spectrometer is not sufficient to select a beam of pure pions. In fact, muons and electrons survive the selection on the beamline mass. It is important to notice that the composition of the negative polarity beam is mostly pions, as will be discussed in section 1.2.1. Anyhow, we devise a selection on the TPC information to mitigate the presence of

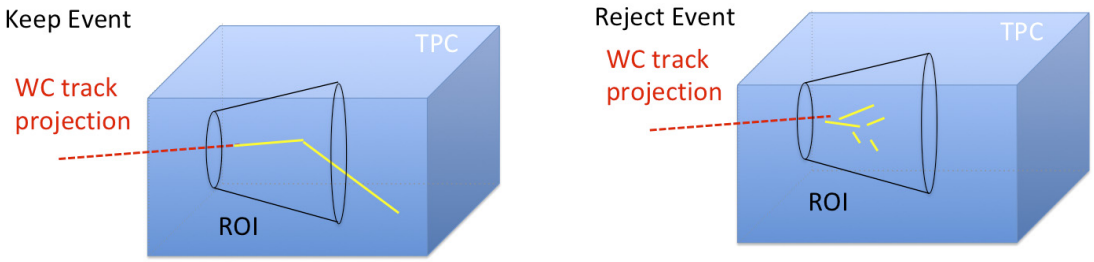

Figure 2: Visual rendering of the shower filter. The ROI is a cut cone, with a small radius of 4 cm, a big radius of 10 cm and an height of 42 cm (corresponding to 3 radiation lengths for electrons in Argon).

electrons in the sample used for the pion cross section. The selection relies on the different topologies of a pion and an electron event in the argon: while the former will trace a track inside the TPC active volume, the latter will tend to "shower", i.e. interact with the medium, producing bremsstrahlung photons which pair convert into several short tracks. In order to remove the shower topology, we create a region of interest (ROI) around the TPC track corresponding to the beamline particle (more details on this in the next section). We look for short tracks contained in the ROI, as depicted in figure 4: if more then 5 tracks shorter than 10 cm are in the ROI, we reject the event. Line 8 in in Table 1) shows the number of events surviving this selection.

0.2 Beamline and TPC Handshake: the Wire Chamber to TPC Match

For each event passing the selection on its beamline information, we need to identify the track inside the TPC corresponding to the particle which triggered the beamline detectors, a procedure we refer to as "WC to TPC match" (WC2TPC for short). In general, the TPC tracking algorithm will reconstruct more than one track in the event, partially due to the fact that hadrons interact in the chamber and partially

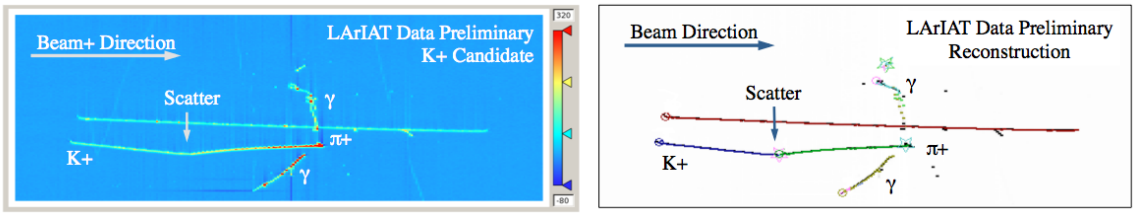

Figure 3: Kaon candidate event: on the right, event display showing raw quantities; on the left, event display showing reconstructed tracks. In the reconstructed event display, different colors represent different track objects. A kink is visible in the kaon ionization, signature of a hadronic interaction: the tracking correctly stops at the kink position and two tracks are formed. An additional pile-up track is so present in the event (top track).

because of pile up particles during the triggered TPC readout time, as shown in figure 3.

We attempt to uniquely match one wire chamber track to one and only one reconstructed TPC track. In order to determine if the presence of a match, we apply a geometrical selection on the relative the position of the wire chamber and TPC tracks. We start by considering only TPC tracks whose first point is in the first 2 cm upstream portion of the TPC for the match. We project the wire chamber track to the TPC front face where we define the coordinates of the projected point as x_{FF} and y_{FF}. For each considered TPC track, we define ΔX as the difference between the x position of the most upstream point of the TPC track and x_{FF}. ΔY is defined analogously. We define the radius difference, ΔR, as $\Delta \mathrm{R} = \sqrt{\Delta \mathrm{X}^2 + \Delta \mathrm{Y}^2}$. We define as α the angle between the incident WC track and the TPC track in the plane that contains them. If $\Delta \mathrm{R} < 4$ cm, $\alpha < 8°$, a match between WC-track and TPC reconstructed track is found. We describe how we determine the value for the radius and angular selection in sec 1.3.3. In MC, we mimic the matching between the WC and the TPC track by constructing a fake WC track using truth information at wire chamber four. We then apply the same WC to TPC matching algorithm as in data. We discard events with multiple WC2TPC matches. We use only those TPC tracks that are matched to WC tracks in the cross section calculation.

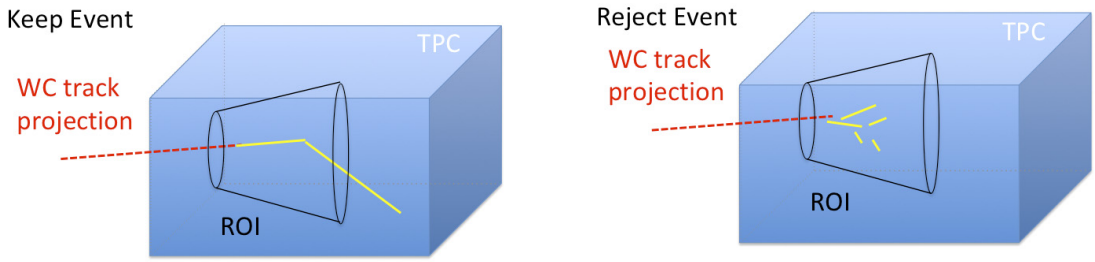

Figure 4: Visual rendering of the wire chamber to TPC match.

0.3 The Thin Slice Method

Once we have selected the pool of hadron candidates and we have identified the TPC track corresponding to the beamline event, we apply the thin slice method to measure the cross section, as the following sections describe.

0.3.1 Cross Sections on Thin Target

Cross section measurements on a thin target have been the bread and butter of nuclear and particle experimentalists since the Geiger-Marsden experiments [**?**]. At their core, these types of experiments consist in shooting a beam of particles with a known flux on a thin target and recording the outgoing flux.

In general, the target is not a single particle, but rather a slab of material containing many diffusion centers. The so-called "thin target" approximation assumes that the target centers are uniformly distributed in the material and that the target is thin compared to the projectile interaction length,WC2TPC so that no center of interaction sits in front of another. In this approximation, the ratio between the number of particles interacting in the target $N_{Interacting}$ and number of incident particles $N_{Incident}$ determines the interaction probability $P_{Interacting}$, which is the complementary to one of the survival probability $P_{Survival}$. Equation 2

$$P_{Survival} = 1 - P_{Interacting} = 1 - \frac{N_{Interacting}}{N_{Incident}} = e^{-\sigma_{TOT} n \delta X} \tag{2}$$

describes the probability for a particle to survive the thin target. This formula relates the total cross section σ_{TOT}, the density of the target centers n and the thickness of the target along the incident hadron direction δX, to the interaction probability[1]. If the target is thin compared to the interaction length of the process considered, we can Taylor expand the exponential function in equation 2 and find a simple proportionality relationship between the number of incident and interacting particles, and the cross section, as shown in equation 3:

$$1 - \frac{N_{Interacting}}{N_{Incident}} = 1 - \sigma_{TOT} n \delta X + O(\delta X^2). \tag{3}$$

Solving for the cross section, we find:

$$\sigma_{TOT} = \frac{1}{n\delta X} \frac{N_{Interacting}}{N_{Incident}}. \tag{4}$$

0.3.2 Not-so-Thin Target: Slicing the Argon

The interaction length of pions and kaons in argon is expected to be of the order of 50 cm for pions and 100 cm for kaons. Thus, the LArIAT TPC, with its 90 cm of length, is not a thin target. However, the fine-grained tracking of the LArIAT LArTPC allows us to treat the argon volume as a sequence of many adjacent thin targets.

As described in Chapter **??**, LArIAT wire planes consist of 240 wires each. The wires are oriented at +/- 60° from the vertical direction at 4 mm spacing, while the beam direction is oriented 3 degrees off the z axis in the XZ plane. The wires collect signals proportional to the energy loss of the hadron along its path in a $\delta X = 4$ mm/sin(60°) $\approx$ 4.7 mm slab of liquid argon. Thus, one can think to slice the TPC

1. The scattering center density in the target, n, relates to the argon density ρ, the Avogadro number N_A and the argon molar mass m_A as $n = \frac{\rho N_A}{m_A}$.

into many thin targets of $\delta X = 4.7$ mm thickness along the direction of the incident particle, making a measurement at each wire along the path.

Considering each slice j a "thin target", we can apply the cross section calculation from Equation 4 iteratively, evaluating the kinetic energy of the hadron as it enters each slice, E_j^{kin}. For each WC2TPC matched particle, the energy of the hadron entering the TPC is known thanks to the momentum and mass determination by the tertiary beamline,

$$E_{FrontFace}^{kin} = \sqrt{p_{Beam}^2 - m_{Beam}^2} - m_{Beam} - E_{loss}, \tag{5}$$

where E_{loss} is a correction for the energy loss in the dead material between the beamline and the TPC front face. The energy of the hadron at each slab is determined by subtracting the energy released by the particle in the previous slabs. For example, at the j^{th} point of a track, the kinetic energy will be

$$E_j^{kin} = E_{FrontFace}^{kin} - \sum_{i<j} \Delta E_i, \tag{6}$$

where ΔE_i is the energy deposited at each argon slice before the j^{th} point as measured by the calorimetry associated with the tracking.

If the particle enters a slice, it contributes to $N_{Incident}(E^{kin})$ in the energy bin corresponding to its kinetic energy in that slice. If it interacts in the slice, it then also contributes to $N_{Interacting}(E^{kin})$ in the appropriate energy bin. The cross section as a function of kinetic energy, $\sigma_{TOT}(E^{kin})$ will then be proportional to the ratio $\frac{N_{Interacting}(E^{kin})}{N_{Incident}(E^{kin})}$.

The statistical uncertainty for each energy bin is calculated by error propagation from the statistical uncertainty on $N_{Incident}$ and $N_{Interacting}$. Since the number of incident hadrons in each energy bin is given by a simple counting, we assume that $N_{Incident}$ is distributed as a poissonian with mean and σ^2 equal to $N_{Incident}$ in each

bin. On the other hand, $N_{Interacting}$ follows a binomial distribution: a particle in a given energy bin might or might not interact. The square of the variance for the binomial is given by

$$\sigma^2 = \mathcal{N} P_{Interacting}(1 - P_{Interacting}); \tag{7}$$

since the interaction probability $P_{Interacting}$ is $\frac{N_{Interacting}}{N_{Incident}}$ and the number of tries $\mathcal{N}$ is $N_{Incident}$, equation 7 translates into

$$\sigma^2 = N_{Incident}\frac{N_{Interacting}}{N_{Incident}}(1 - \frac{N_{Interacting}}{N_{Incident}}) = N_{Interacting}(1 - \frac{N_{Interacting}}{N_{Incident}}). \tag{8}$$

$N_{Incident}$ and $N_{Interacting}$ are not independent. The uncertainty on the cross section is thus calculated as

$$\delta\sigma_{tot}(E) = \sigma_{tot}(E)\Big(\frac{\delta N_{Interacting}}{N_{Interacting}} + \frac{\delta N_{Incident}}{N_{Incident}}\Big) \tag{9}$$

where:

$$\delta N_{Incident} = \sqrt{N_{Incident}} \tag{10}$$

$$\delta N_{Interacting} = \sqrt{N_{Interacting}\Big(1 - \frac{N_{Interacting}}{N_{Incident}}\Big)}. \tag{11}$$

0.3.3 Corrections to the Raw Cross Section

Equation 4 is a prescription for measuring the cross section in case of a pure beam of the hadron of interest and 100% efficiency in the determination of the interaction point. For example, if LArIAT had a beam of pure pions and were 100% efficient in determining the interaction point within the TPC, the pion cross section in each energy bin would be given by

$$\sigma^{\pi^-}(E_i) = \frac{1}{n\delta X}\frac{N^{\pi^-}_{\text{Interacting}}(E_i)}{N^{\pi^-}_{\text{Incident}}(E_i)}. \tag{12}$$

Unfortunately, this is not the case. In fact, the selection used to isolate pions in the LArIAT beam allows for the presence of some muons and electrons as background. Also, the LArIAT TPC is not 100% efficient in determining the interaction point. Therefore we need to apply two corrections evaluated on the MC in order to extract the cross section from LArIAT data: the background subtraction and the efficiency correction. Still using the pion case as example, we estimate the pion cross section in each energy bin changing Equation 12 into

$$\sigma^{\pi^-}(E_i) = \frac{1}{n\delta X}\frac{N^{\pi^-}_{\text{Interacting}}(E_i)}{N^{\pi^-}_{\text{Incident}}(E_i)} = \frac{1}{n\delta X}\frac{\epsilon_i^{inc}[N^{\text{TOT}}_{\text{Interacting}}(E_i) - B_{\text{Interacting}}(E_i)]}{\epsilon_i^{int}[N^{\text{TOT}}_{\text{Incident}}(E_i) - B_{\text{Incident}}(E_i)]}, \quad (13)$$

where $N^{\text{TOT}}_{\text{Interacting}}(E_i)$ and $N^{\text{TOT}}_{\text{Incident}}(E_i)$ is the measured content of the interacting and incident histograms for events that pass the event selection, $B_{interacting}(E_i)$ and $B_{\text{Incident}}(E_i)$ represent the contributions from beamline background, and ϵ_i^{int} and ϵ_i^{inc} are the efficiency corrections for said histograms.

As we will show in section **??**, the background subtraction for the interacting and incident histograms can be translated into a corresponding corrections $C^{\pi MC}_{Interacting}(E_i)$ and $C^{\pi MC}_{Incident}(E_i)$ and the cross section re-written as follows

$$\sigma^{\pi^-}(E_i) = \frac{1}{n\delta X}\frac{\epsilon_i^{inc}\ N^{\text{TOT}}_{\text{Interacting}}(E_i)\ C^{\pi MC}_{Interacting}(E_i)}{\epsilon_i^{int}\ N^{\text{TOT}}_{\text{Incident}}(E_i)\ C^{\pi MC}_{Incident}(E_i)}. \quad (14)$$

0.4 Procedure testing with truth quantities

The (π^-,Ar) and (K^+,Ar) total hadronic cross section implemented in Geant4 can be used as a tool to validate the measurement methodology. We describe here a closure test done on Monte Carlo to prove that the methodology of slicing the TPC retrieves the underlying cross section distribution implemented in Geant4 within the statistical uncertainty.

For pions in the considered energy range, the Geant4 inelastic model adopted to

is "BertiniCascade", while the elastic model "hElasticLHEP". For kaons, the Geant4 inelastic model adopted to is "BertiniCascade", while the elastic model "hElasticLHEP".

For the validation test, we fire about a sample of pions and a sample of kaons inside the LArIAT TPC active volume using the Data Driven Monte Carlo (see section 1.2.2). We apply the thin-sliced method using only true quantities to calculate the hadron kinetic energy at each slab in order to decouple reconstruction effects from issues with the methodology. For each slab of 4.7 mm length along the path of the hadron, we integrate the true energy deposition as given by the Geant4 transportation model. Then, we recursively subtracted it from the hadron kinetic energy at the TPC front face to evaluate the kinetic energy at each slab until the true interaction point is reached. Since the MC is a pure beam of the hadron of interest and truth information is used to retrieve the interaction point, no correction is applied. Doing so, we obtain the true interacting and incident distributions for the considered hadron and we obtain the true MC cross section as a function of the hadron true kinetic energy.

Figure 5 shows the total hadronic cross section for argon implemented in Geant4 10.01.p3 (solid lines) overlaid with the true MC cross section as obtained with the sliced TPC method (markers) for pions on the left and kaons on the right; the total cross section is shown in green, the elastic cross section in blue and the inelastic cross section in red. The nice agreement with the Geant4 distribution and the cross section obtained with the sliced TPC method gives us confidence in the validity of the methodology.

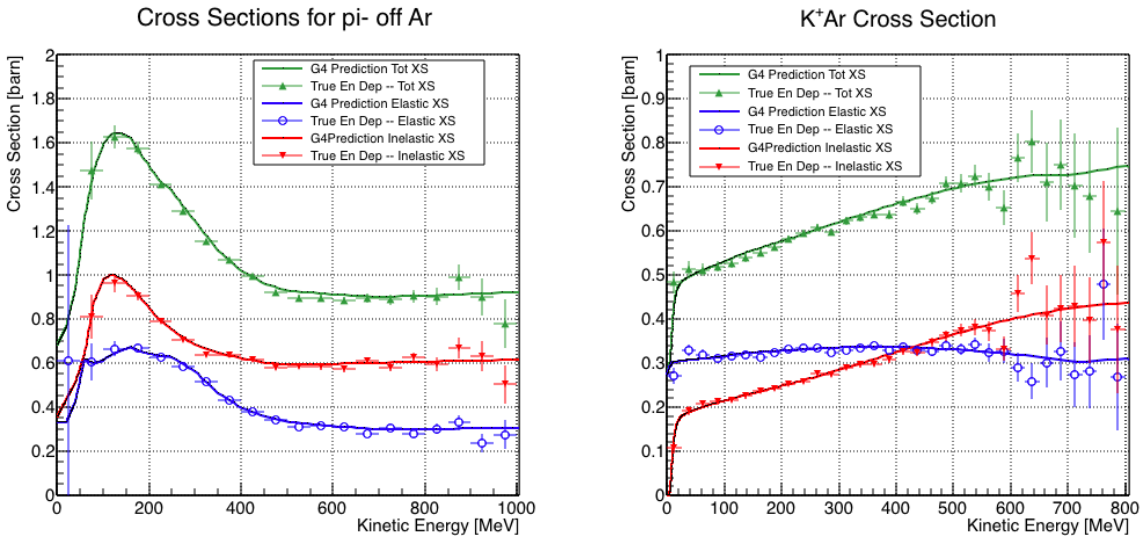

Figure 5: Hadronic cross sections for (π^-,Ar) on the left and (K^+,Ar) on the right as implemented in Geant4 10.01.p3 (solid lines) overlaid the true MC cross section as obtained with the sliced TPC method (markers). The total cross section is shown in green, the elastic cross section in blue and the inelastic cross section in red.

Chapter 1

Preparatory Work

This chapter describes the preparatory work done on the the data and Monte Carlo samples used for the cross section analyses. This entails the choice of the data set and the production of the information needed to construct the Monte Carlo Simulation (section 1.1), the construction and use of said Monte Carlo simulation (section 1.2), the study and optimization of the tracking in the TPC for the cross section analyses (section 1.3), the calibration of the calorimetry response and related energy studies (section 1.4).

1.1 Cross Section Analyses Data Set

We choose LArIAT Run-II as the data period for the (π^-,Ar) and (K^+,Ar) total hadronic cross section analyses. Data taking for the this period started on 03/15/2016 and ended on 07/31/2016. Since we are interested in beamline and TPC information, we ask basic requirements on the operational status of the time of fight, wire chambers and TPC to form the good run list for this period, which we informally call "lovely runs".

The subset of lovely runs chosen for the (π^-,Ar) total hadronic cross section analysis includes only the -60A and -100A magnet configurations in negative polarity,

even if LArIAT explored several other beamline configurations during Run-II. The -60A and -100A combined data set accounts for approximately 90% of the total Run-II negative polarity runs. Since the production of beamline Monte Carlo depends on the wanted beamline configuration, the choice of only two beamline settings limits the need for beamline MC production.

Similarly, the subset of lovely runs chosen for the (K^+,Ar) total hadronic cross section analysis includes only the +60A and +100A magnet configurations in positive polarity. It should be noted that kaons are extremely rare in the +60A sample, thus the data sample for the (K^+,Ar) cross section after the mass selection is about 90% +100A runs, as shown in Table 1.1.

For the first measurements in LArIAT that uses both beamline and TPC information, we choose strict requirements on the reconstruction of the WC tracks, the so-called "Picky Track" sample (see **??**). This choice presents two advantages: the uncertainty on the momentum reconstruction for the "Picky Tracks" sample is smaller compared to the "High Yield" sample, and the comparison with the beamline MC results is straightforward. A possible future update and cross check of these analysis would be the use of the High Yield sample, where the statistics is about three times higher.

The breakdown of beamline events as a function of the magnets settings is shown in Table 1.1. The choice of the data sets determines the production of beamline MC and serves as basis for the production of Data Driven MC, as shown in the next sections.

	I = 60 A	I = 100 A	Total
Data Events after $\pi/\mu/e$ Mass Selection	67068	71413	138481
Data Events after K Mass Selection	274	2563	2837

Table 1.1: Number of data events which fit the $\pi/\mu/e$ or K mass hypothesis as a function of magnet settings.

1.2 Construction of a Monte Carlo Simulation for LArIAT

For the simulation of LArIAT events and their particle make up, we use a combination of two MC generators: the G4Beamline Monte Carlo and the Data Driven single particle Monte Carlo (DDMC). We use the G4Beamline MC to simulate the particle transportation in the beamline and calculate the particle composition of the beam just after the fourth Wire Chamber (WC4). In order to simulate the beamline particles after WC4 and in the TPC, we use the DDMC.

1.2.1 G4Beamline

G4Beamline simulates the beam collision with the LArIAT secondary target, the energy deposited by the particles in the LArIAT beamline detectors, and the action of the LArIAT magnets, effectively accounting for particle transportation through the beam line from the LArIAT target until "Big Disk", a fictional, void detector located just before the LArIAT cryostat. At the moment of this writing, G4Beamline does not simulated the responses of the beam line detectors. It is possible to interrogate the truth level information of the simulated particles in several points of the geometry. In order to ease the handshake between G4Beamline and the DDMC, we ask for the beam composition just after WC4. Since LArIAT data are taken under different beam conditions, we need to simulate separately the beam composition according to the magnets' settings and the secondary beam intensity with G4Beamline. For the pion cross section analysis the relevant beam conditions are secondary beam energy of 64 GeV, negative polarity magnet with current of 100 A and 60 A. For the kaon cross section analysis the relevant beam conditions is a secondary beam energy of 64 GeV, positive polarity magnet with current of 100 A.

	I = -60 A	I = -100 A
G4Pions	68.8 %	87.4 %
G4Muons	4.6 %	3.7 %
G4Electrons	26.6 %	8.9 %

Table 1.2: Simulated beamline composition per magnet settings

Beam Composition for Negative Pion Cross Section

Even if pions are by far the biggest beam component in negative polarity runs, the LArIAT tertiary beam is not a pure pion beam. While useful to discriminate between pions, kaons, and protons, the beamline detectors are not sensitive enough to discriminate among the lighter particles in the beam: electrons, muons and pions fall under the same mass hypothesis. Thus, we need to assess the contamination from beamline particles other than pions in the event selections used for the pion cross section analysis and correct for its effects. The first step of this process is assessing the percentage of electrons and muons in the $\pi/\mu/e$ beamline candidates via the G4Beamline MC. The full treatment of the beamline contamination in the pion cross section calculation is described in section 2.2. Since the beamline composition is a function of the magnet settings, we simulate separately events for magnet current of -60A and -100A. Figure 1.1 shows the momentum predictions from G4Beamline overlaid with data for the 60A runs (left) and for the 100A runs (right). The predictions for electrons, muons and pions have been staggered and their sum is area normalized to data. Albeit not perfect, these plots show a reasonable agreement between the momentum shapes in data and MC. We attribute the difference in shape to the lack of simulation of the WC efficiency in the MC which is momentum dependent and leads to enhance the number events in the center of the momentum distribution.

Table 1.2 shows the beam composition per magnet setting after the mass selection according to the G4Beamline simulation.

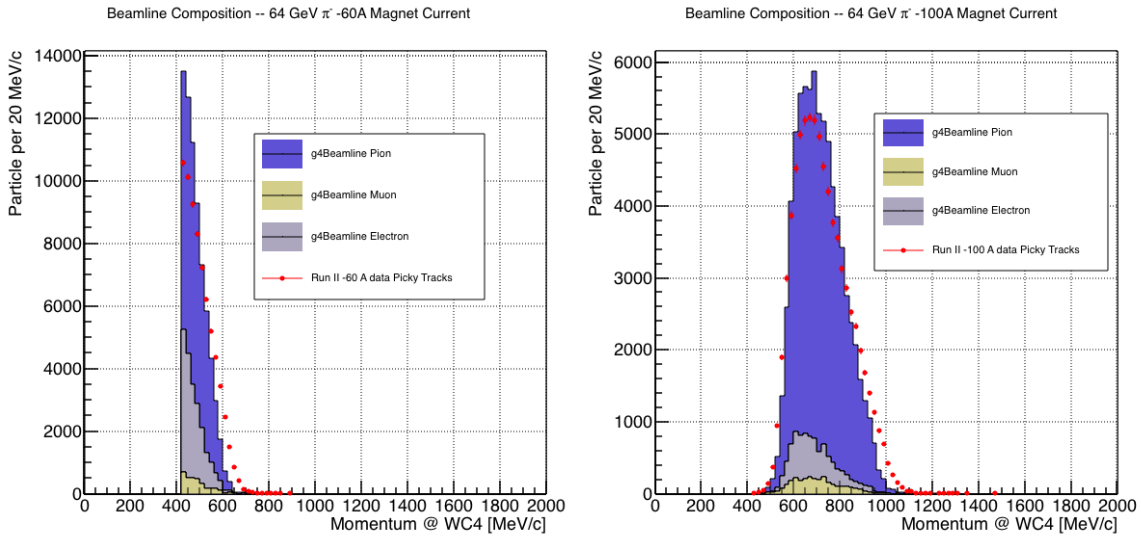

Figure 1.1: Beam composition for the -60A runs (left) and -100A runs (right). The solid blue plot represents the simulated pion content, the yellow plot represents the simulated muon content and the grey plot represents the simulated electron content. The plots are area normalized to the number of data events, shown in red.

Beam Composition for Positive Kaon Cross Section

In the positive polarity runs, the tertiary beam composition is mainly pions and protons. The left side of Figure 1.2 shows the predictions for the momentum spectra for the 100A positive runs according to G4Beamline (solid colors) overlaid with data (black points). Since the LArIAT beamline detectors can discriminate between kaons and other particles, we do not rely on the G4Beamline simulation to estimate the beamline contamination in the pool of kaon candidates (as in the case of the pion cross section), but rather we use a data drive approach. The basic idea of this data driven approach is to estimate the bleed over from high and low mass peaks under the kaon peak by fitting the tails of the $\pi/\mu/e$ and proton mass distributions, as shown in Figure 1.2 right side. Since the shape of the tails is unknown, the estimate is done multiple times varying the range and shape for reasonable functions. For example, to estimate the proton content under the kaon peak, we start by fitting the left tail of the proton mass distribution with a gaussian function between 650 MeV/c^2 and 750

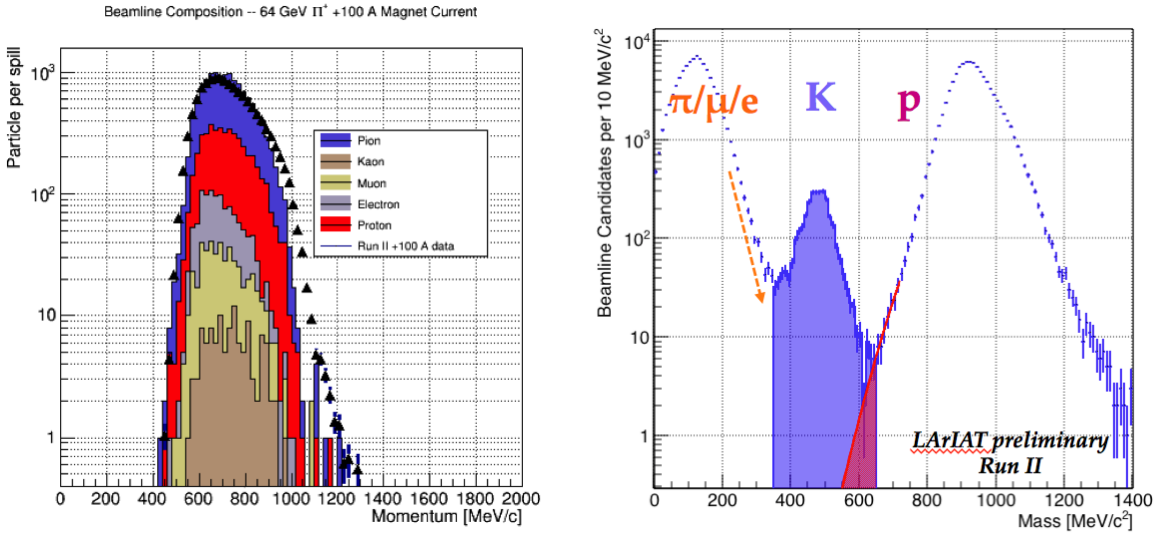

Figure 1.2: *Left*. Beam composition for the +100A runs after WC4 (no mass selection applied). The solid blue plot represents the simulated pion content, the yellow plot represents the simulated muon content and the grey plot represents the simulated positron content, the red the proton content and the mustard the kaon content. The plots are area normalized to the number of data events, shown in black.*Right*. Mass distribution for the Run-II positive runs, where the area under the kaon mass peak is highlighted in purple. The area under the extension of a possible fit for the proton tail is highlighted in red.

MeV/c^2.We extend the fit function under the kaon peak and integrate the between 350-650 MeV/c^2. We integrate the mass histogram in the same range and calculate the proton contamination as the ratio between the two integrals. We repeat this procedure for several fit shapes (gaussian, linear and exponential functions are used) and tail ranges. Finally, we calculate the contamination as the weighted average of single estimates, where the weights are calculated to be the $1./\chi^2$ of the tail fits. The procedure is repeated for lighter particles mass peak independently. With 12 iterations of this method we find a proton contamination of 0.2 $\pm$ 0.5 % and a contamination from the lighter particles of 5 $\pm$ 2 % .

1.2.2 Data Driven MC

The Data Driven single particle Monte Carlo (DDMC) is a single particle gun which simulates the particle transportation from WC4 into the TPC leveraging on the beamline data information. The DDMC uses the data momentum and position at WC4 to derive the event generation: a general sketch of the DDMC workflow is shown in Figure 1.3.

When producing a DDMC sample, beam line data from a particular running period and/or running condition are selected first. For example, data for the negative 60A runs and for the negative 100A runs inform the event generation stage of two different DDMC samples. Figure 1.4 schematically shows the data quantities of interest leveraged from data: the momentum (P_x, P_y, P_z) and position (X, Y) at WC4. For each data event, we obtain the particle position (X, Y) at WC4 directly from the data measurement; we calculate the components of the momentum using the beamline measurement of the momentum magnitude in conjunction with the hits on WC3 and WC4 to determine the direction of the momentum vector, as described in section **??**. The momentum and position of the selected data form a 5-dimensional tupla, which we sample thousands of times through a 5-dimensional hit-or-miss sampling procedure to generate the MC events. This produces MC P_x, P_y, P_z, X, Y distributions with the same momentum and position distributions as data, with the additional benefit of accounting for the correlations between the considered variables. As an example, the results of the DDMC generation compared to data for the kaon +100A sample are shown in figure **??** for the P_z, X and Y distributions; as expected, MC and data agree within the statistical uncertainty by construction. A LArSoft simulation module then launches single particle MC from z = -100 cm (the location of the WC4) using the MC generated events. The particles are free to decay and interact in their path from WC4 to the TPC according to the Geant4 simulation.

Using the DDMC technique ensures that the MC and data particles have very

similar momentum, position and angular distributions at WC4 and allows us to use the MC sample in several occasions, for example to calibrate the energy loss upstream of the TPC (see Section 1.2.3) or to study the tracking and the calorimetric performance (sections 1.3 and 1.4). A small caveat is in order here: the DDMC is a single particle Monte Carlo, which means that the beam pile-up is not simulated.

Six samples are the basis fo the MC used in the pion cross section measurement: three samples of ∼340000 pions, muons and electrons to simulate the negative 60A runs, and three samples of ∼340000 pions, muons and electrons for the negative 100A runs.

The MC used for the kaon cross section analysis is a sample of NUMBERS kaons.

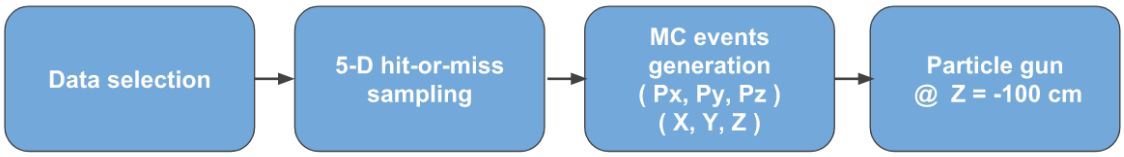

Figure 1.3: Workflow for Data Driven single particle Monte Carlo production.

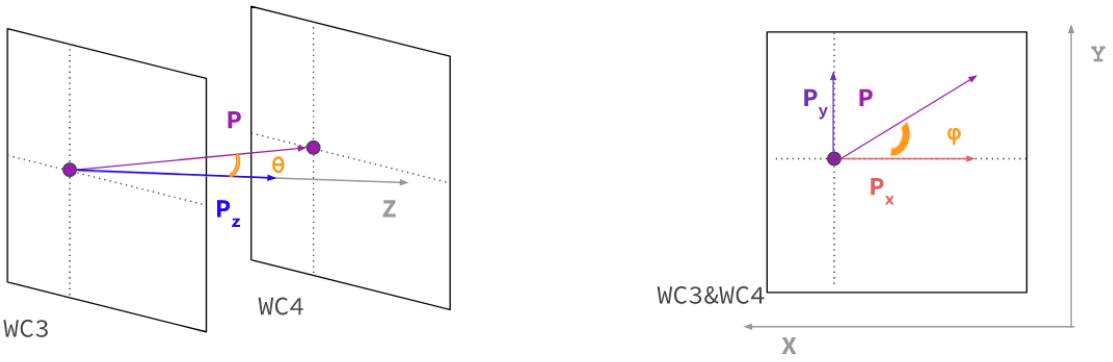

Figure 1.4: Scheme of the quantities of interest for the DDMC event generation: P_x, P_y, P_z, X, Y at WC4.

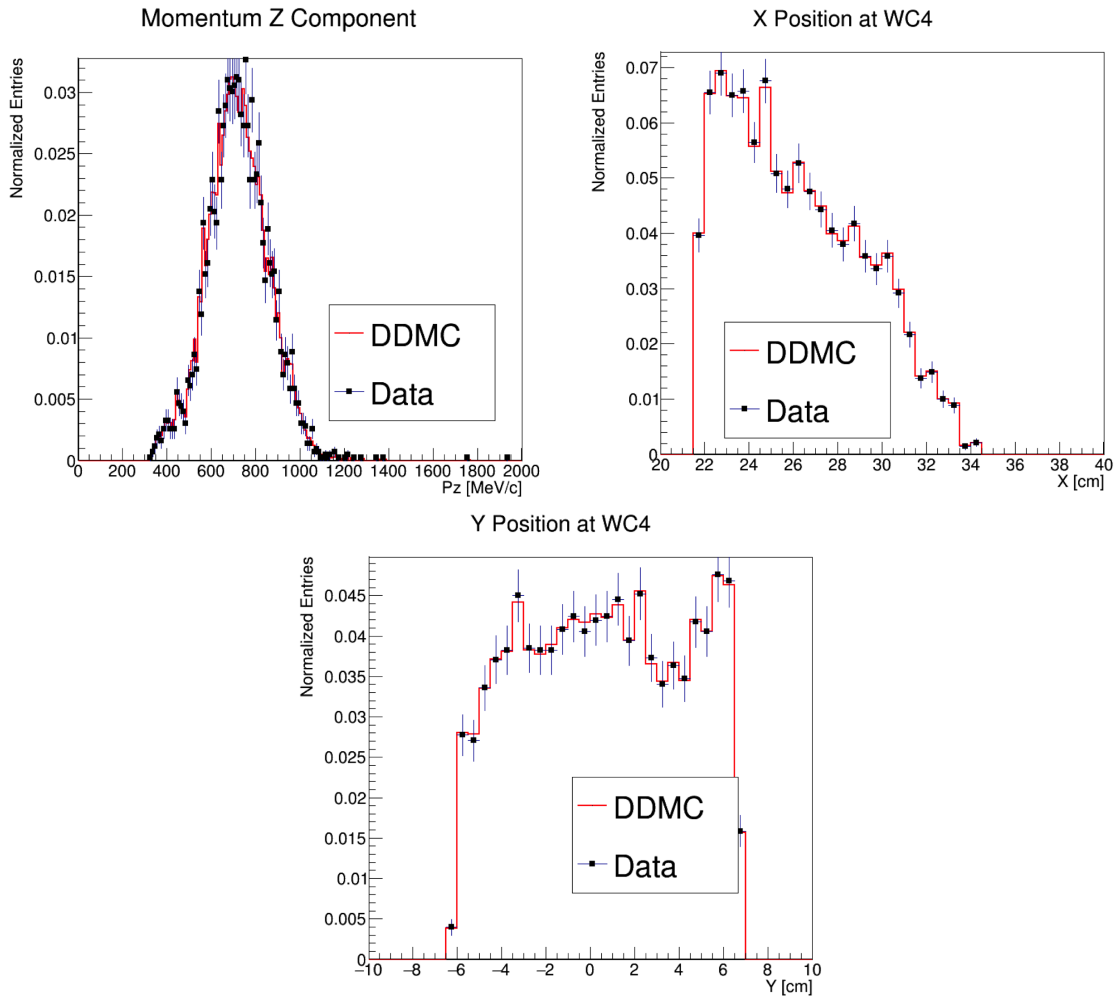

Figure 1.5: Comparison between generated quantities and data distributions for the 100A kaon sample: Z component of the momentum at WC4 (top left), X position at Wire Chamber 4 (top right), Y position at Wire Chamber 4 (bottom).

1.2.3 Estimate of Energy Loss before the TPC

The beamline particles travel a path from where their momentum is measured in the beamline until they are tracked again inside the TPC. In the LArIAT geometry, a particle leaving the WC4 will encounter the materials listed in Table 1.3 before being registered again. The energy lost by the particle in this non-instrumented material modifies the particle's kinetic energy and directly affects the cross section measurement, as shown in equation 5.

Material	density [g/cm^3]	width [cm]
Fiberglass laminate (G10)	1.7	1.28
Liquid Argon	1.4	3.20
Stainless Steel	7.7	0.23
Titanium	4.5	0.04
Air	1.2 $\cdot 10^{-3}$	89.43
Plastic Scintillator	1.03	1.20 (+ 1.30)

Table 1.3: LArIAT material budget from WC4 to the TPC Front Face.

We derive an estimate of the energy loss between the beamline momentum measurement and the TPC (E_{loss}) from the pion DDMC sample, since this quantity is not measurable directly on data. The E_{loss} distribution for the 60A and 100A pion sample is shown in figure 1.6, left and right respectively. A clear double peaked structure is visible, which is due to the particles either missing or hitting the HALO paddle: a schematic rendering of this occurrence is shown in figure 1.7. The kinematic at WC4 determines the trajectory of a particle and whether or not it will hit the halo paddle. In figure 1.8 , we plot the true horizontal component of the momentum P_x versus the true X position at WC4 for pions missing the halo paddle (left) and for pions hitting the halo paddle (right) for the 60A MC simulation runs – analogous plots are obtained with the 100A simulation. These distributions can be separated drawing a line in this position-momentum space. We use a logistic regression [**?**] as a classifier to find the best separating line, shown in both plots as the red line. We classify as

"hitting the halo paddle" all pions whose P_x and X are such that

$$P_x + 0.02 * X - 0.4 < 0$$

and as "missing the halo paddle" all pions whose P_x and X are such that

$$P_x + 0.02 * X - 0.4 > 0,$$

where the coefficients of the line are empirically found by the logistic regression estimation. Overall, this simple methode classifies in the right category (hit or miss) about 86% of the pion events. In MC, we assign $E_{loss} = 32 \pm 4$ MeV for pion events classified as "hitting the halo paddle"; we assign $E_{loss} = 24 \pm 3$ MeV for pion events classified as "missing the halo paddle". We apply the same classifier on data. A scan of the simulated geometry showed an excess of 3 cm of un-instrumented argon compared with the surveyed detector geometry. We account for this difference by assigning in data $E_{loss} = 24 \pm 6$ MeV for pion events classified as "hitting the halo paddle" and $E_{loss} = 17 \pm 6$ MeV for pion events classified as "missing the halo paddle", where the uncertainty is derived as the standard deviation of the double peaked distribution.

The summary of the values for used for E_{Loss} for the pion sample is listed in table 1.4 with the analogous results for the study on the kaon case.

	E_{loss} [MeV]	
	Hitting Halo	Missing Halo
Pion MC	32 ± 4	24 ± 3
Pion Data	25 ± 6	17 ± 6
Kaon MC	37 ± 5	31 ± 4
Kaon Data	26 ± 6	22 ± 6

Table 1.4: Energy loss for pions and kaons.

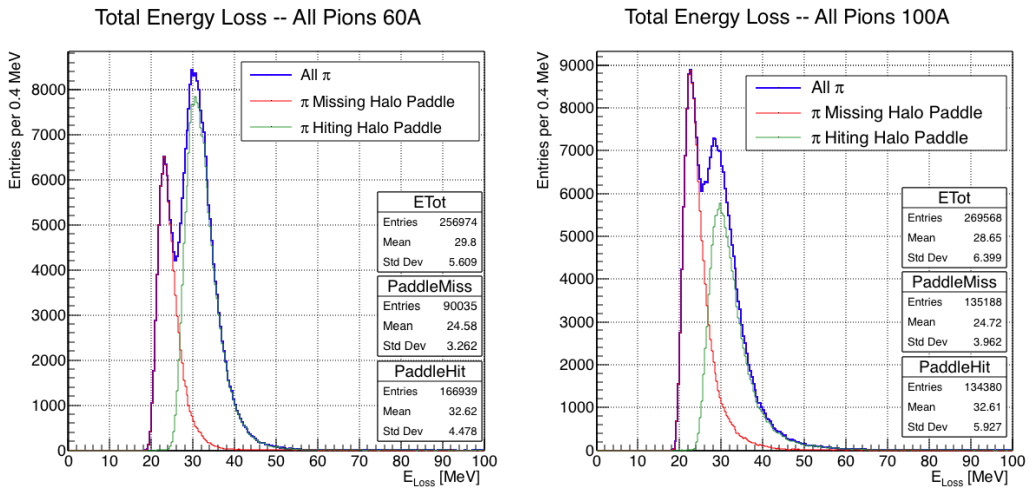

Figure 1.6: True energy loss between WC4 and the TPC front face according to the MC simulation of negative pions of the 60A runs (left) and of the 100A runs (right). The distribution for the whole data sample is shown in blue, the distribution for the pions missing the halo is shown in red, and the distribution for the pions hitting the halo is shown in green.

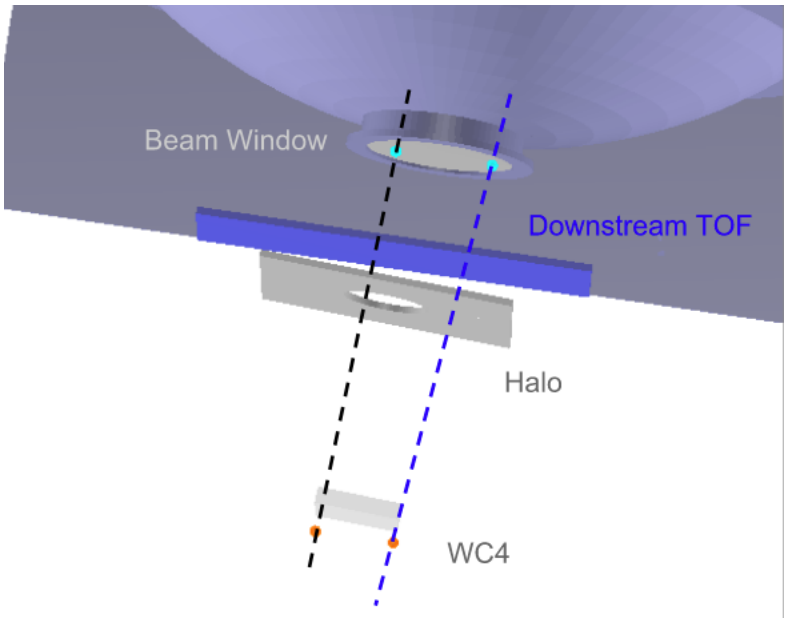

Figure 1.7: Schematic rendering of the particle path between WC4 and the TPC front face. The paddle with the hollow central circle represents the Halo paddle. We illustrate two possible trajectories: in black, a trajectory that miss the paddle and goes through the hole in the Halo, in blue a trajectory that hits the Halo paddle and goes through the scintillation material.

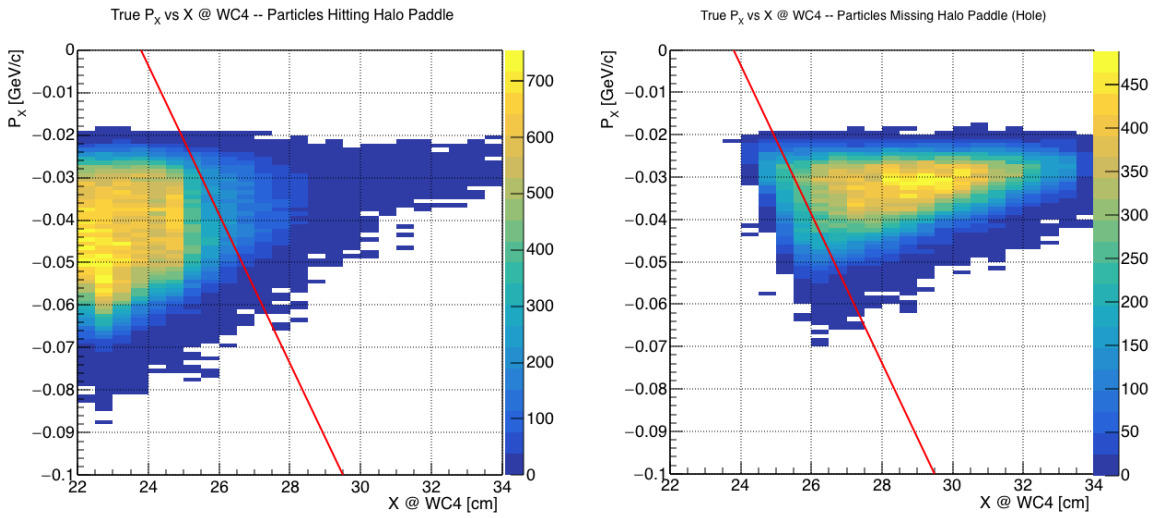

Figure 1.8: Horizontal component of the true momentum vs the horizontal position at WC4 for MC simulated pions of the 60A runs. The plot on the left shows the distribution for pion that miss the halo paddle and the plot on the right shows the distributions for pions that hit the halo. The form of the classifier is overlaid to both plots (red line).

1.3 Tracking Studies

In this section, we describe three studies. The first is a justification of the selection criteria for the beamline handshake with the TPC information. We perform this study to boost the correct identification of the particles in the TPC associated with the beamline information, while maintaining sufficient statistics for the cross section measurement. The second study is an optimization of the tracking algorithm, with the scope of maximizing the identification of the hadronic interaction point inside the TPC. These two studies are related, since the optimization of the tracking is performed on TPC tracks which have been matched to the wire chamber track; in turn, the tracking algorithm for TPC tracks determines the number of reconstructed tracks in each event used to try the matching with the wire chamber track. Starting with a sensible tracking reconstruction, we perform the WC2TPC matching optimization first, then the tracking optimization. The WC2TPC match purity and efficiency are then calculated again with the optimized tracking. The third study is an evaluation of

the angular resolution of the tracking algorithm in data and MC, which is particularly important in the context of the cross section analyses.

1.3.1 Study of WC to TPC Match

1.3.2 Tracking Optimization

1.3.3 Study of WC to TPC Match

1.3.4 Angular Resolution

Scope of this study is to understand and compare the tracking performances and angular resolution of the TPC tracking on data and MC. We use the angular resolution of the tracking to determine the value of smallest angle that we can reconstruct with a non-zero efficiency, effectively determining a selection on the angular distribution of the cross section measurement due to the tracking performance.

We start by selecting all the WC2TPC matched tracks used for the cross section analysis. These tracks can contain from a minimum of 3 3D-space points to a maximum of 240 3D-space points. We fit a line to all the 3D-space points associated with the track. For each track we calculate the average distance between each point in space and the fit line as follows

$$\bar{d} = \frac{\sum_i^N d_i}{N}, \tag{1.1}$$

where N is the number of 3D-space points of the track and d_i is the distance of the i-th space point to the line fit. Several tests to compare the goodness of fit between data and MC have been considered. We decided to use $\bar{d}$ for its straightforward interpretation. The $\bar{d}$ distribution for data and MC is shown in Figure 1.9 and shows a relatively good agreement between data and MC.

A visual representation of the procedure used to evaluate the angular resolution is shown in Figure 1.11. For each track, we order the space points according to their Z

position along the positive beam direction (panel a) and we split them in two sets: the first set contains all the points belonging to the first half of the track and the second set contains all the points belonging the second half of the track. We remove the last four points in the first set and the first four points in the second set, so to have a gap in the middle of the original track (panel b). We fit the first and the second set of points with two lines (panel c). We then calculate the angle between the fit of the first and second half α (panel d). The angle α determines the spatial resolution of the tracking. The distributions for data and MC for α are given in Figure 1.10. The mean of the data and MC angular resolution are respectively

$$\bar{\alpha}_{Data} = (5.0 \pm 4.5) \text{ deg} \tag{1.2}$$

$$\bar{\alpha}_{MC} = (4.5 \pm 3.9) \text{ deg}. \tag{1.3}$$

Interaction angles smaller than the angle resolution are indistinguishable for the reconstruction. Therefore, we assess our ability to measure the cross section to be limited to interaction angles greater than 5.0 deg. More accurate studies of the angular resolution as a function of the kinetic energy and track length, albeit interesting, are left for an improvement of the analysis.

It is beneficial to take a moment to describe the definition of interaction angle. In case of elastic scattering, the definition is straightforward: the interaction angle is the angle between the incoming and outgoing pion, i.e.

$$\theta = \cos^{-1}\left(\frac{\vec{p}_{\text{incoming}} \cdot \vec{p}_{\text{outgoing}}}{|\vec{p}_{\text{incoming}}||\vec{p}_{\text{outgoing}}|}\right). \tag{1.4}$$

In case of inelastic scattering, the presence of several topologies requires a more complex definition, as shown in figure 1.12. We define the scattering angle as the biggest of the angles between the incoming pion and the visible daughters, where the

visible daughters are charged particles that travel more than 0.47 cm in the detector (see panel a); in case all the daughters are invisible, the angle is assigned to be 90 deg (see panel b). We chose this working definition of scattering angle for inelastic scattering keeping in mind how our tracking reconstruction works: the tracking will stop correctly in case of all the daughters are not visible in the detector and it is likely to stop correctly if multiple daughters form an interaction vertex. The only "dangerous" case is the production of one charged daughter plus neutrals, which we can study with this working definition of scattering angle (see panel c).

We can see the effects of the angular resolution on the cross section by plotting the true Geant4 cross section for interaction angles greater than a minimum interaction angle. Figure 1.13 shows the true Geant4 cross section for interaction angles greater than 0 deg (green), 4.5 deg (red), 5.0 deg (blue) and 9.0 deg (yellow). A small 0.5 deg systematic shift between the mean of the data and MC angular resolution is present.

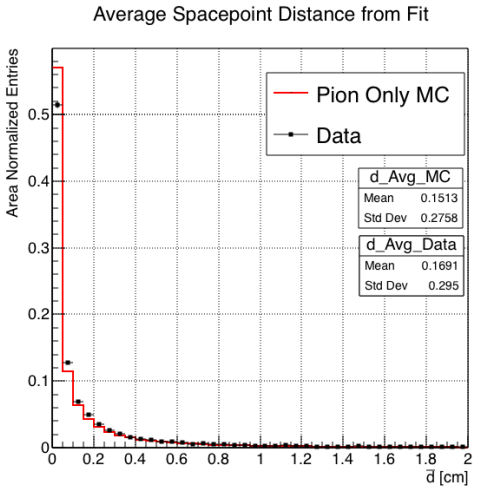

Figure 1.9: Distributions of the average distance between each 3D point in space and the fit line, $\bar{d}$ for the data used in the pion cross section analysis and the pion only DDMC. The distributions are area normalized.

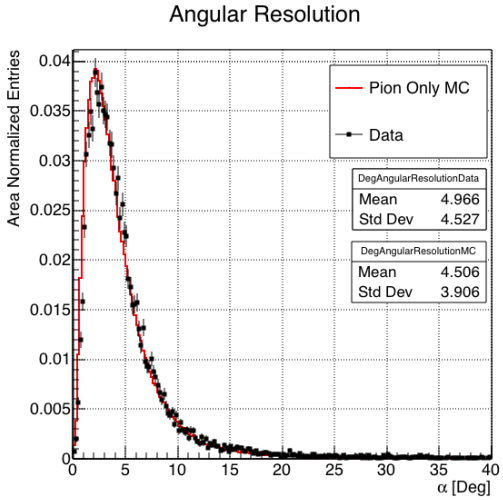

Figure 1.10: Distributions of angular resolution α for data used in the pion cross section analysis and pion only DDMC. The distributions are area normalized.

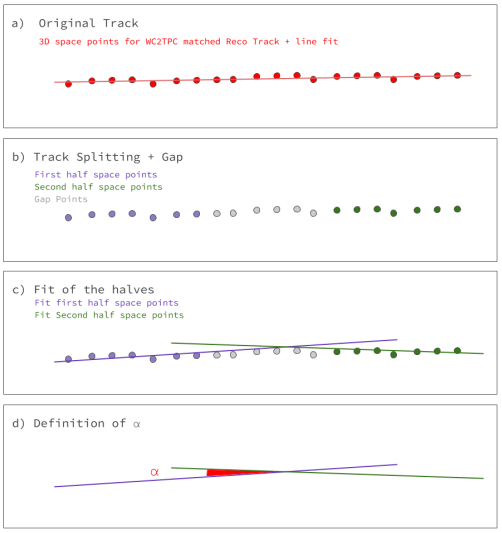

Figure 1.11: A visual representation of the procedure used to evaluate the angular resolution.

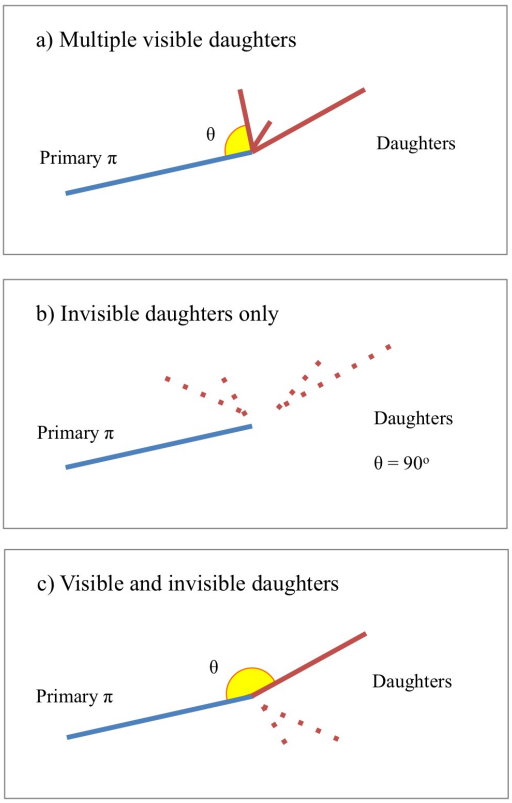

Figure 1.12: A visual representation of the scattering angle definition in case of inelastic scattering.

1.4 Energy Calibration and Studies

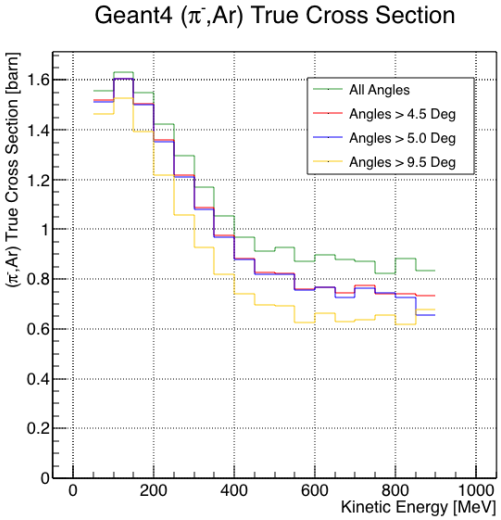

Figure 1.13: True $(\pi^- -, Ar)$ cross section for interaction angles greater than 0 deg (green), 4.5 deg (red), 5.0 deg (blue) and 9.0 deg (yellow).

Chapter 2

Negative Pion Cross Section Measurement

2.1 Raw Cross Section

2.2 Background Subtracted Cross Section

2.3 Efficiency Corrected Cross Section

Chapter 3

Positive Kaon Cross Section Measurement

3.1 Raw Cross Section

Appendix A

Measurement of LArIAT Electric Field

The electric field of a LArTPC in the drift volume is a fundamental quantity for the proper functionality of this technology, as it affects almost every reconstructed quantity such as the position of hits or their collected charge. Given its importance, we calculate the electric field for LArIAT with a single line diagram from our HV circuit and we cross check the obtained value with a measurement relying only on TPC data.

Before getting into the details of the measurement procedures, it is important to explicit the relationship between some quantities in play. The electric field and the drift velocity (v_{drift}) are related as follows

$$v_{drift} = \mu(E_{field}, T)E_{field}, \tag{A.1}$$

where μ is the electron mobility, which depends on the electric field and on the temperature (T). The empirical formula for this dependency is described in [**?**] and shown in Figure A.1 for several argon temperatures.

The relationship between the drift time (t_{drift}) and the drift velocity is trivially

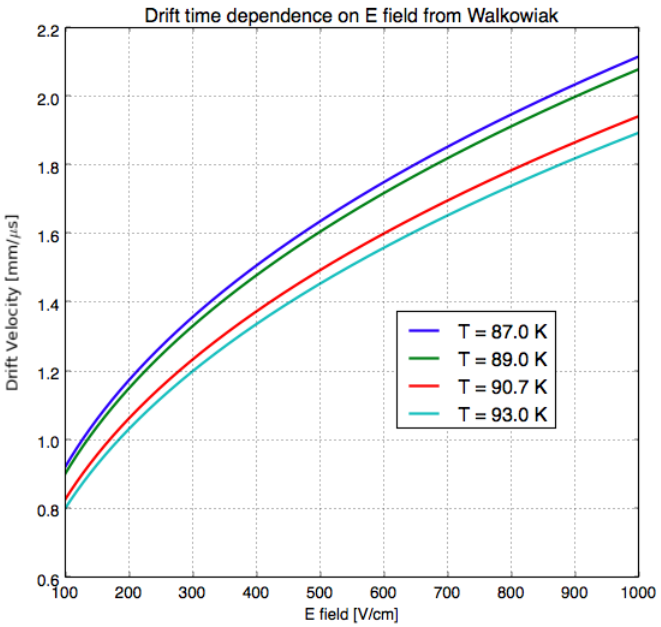

Figure A.1: Drift velocity dependence on electric field for several temperatures. The slope of the line at any one point represents the electron mobility for that given temperature and electric field.

Table A.1: Electric field and drift velocities in LArIAT smaller drift volumes

	Shield-Induction	Induction-Collection
E_{field}	700.63 V/cm	892.5 V/cm
v_{drift}	1.73 mm/μs	1.90 mm/μs
t_{drift}	2.31 μs	2.11 μs

given by

$$t_{drift} = \Delta x / v_{drift}, \tag{A.2}$$

where Δx is the distance between the edges of the drift region. Table A.1 reports the values of the electric field, drift velocity, and drift times for the smaller drift volumes.

With these basic parameters established, we can now move on to calculating the electric field in the main drift region (between the cathode and the shield plane).

Single line diagram method

The electric field strength in the LArIAT main drift volume can be determined knowing the voltage applied to the cathode, the voltage applied at the shield plane, and the distance between them. We assume the distance between the cathode and the shield plane to be 470 mm and any length contraction due to the liquid argon is negligibly small (∼2 mm).

The voltage applied to the cathode can be calculated using Ohm's law and the single line diagram shown in Figure A.2. A set of two of filter pots for emergency power dissipation are positioned between the Glassman power supply and the cathode, one at each end of the feeder cable, each with an internal resistance of 40 MΩ.

Given the TPC resistor chain, the total TPC impedance is 6 GΩ. Since the total resistance on the circuit is driven by the TPC impedance, we expect the resulting current to be

$$I = V_{PS}/R_{tot} = -23.5 \text{ kV}/6 \text{ G}\Omega \sim 4 \ \mu\text{A}, \tag{A.3}$$

which we measure with the Glassman power supply, shown in Figure A.3.

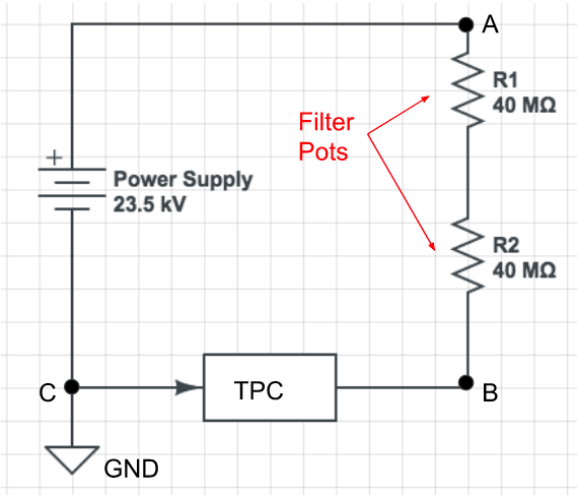

Figure A.2: LArIAT HV simple schematics.

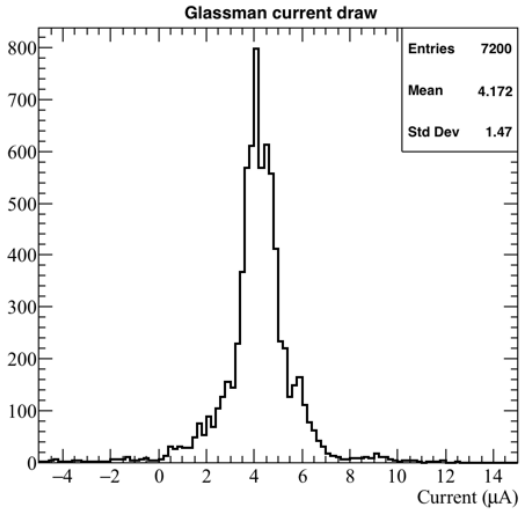

Figure A.3: Current reading from the Glassman between May 25th and May 30th, 2016 (typical Run-II conditions).

Using this current, the voltage at the cathode is calculated as

$$V_{BC} = V_{PS} - (I \times R_{eq}) = -23.5 \text{ kV} + (0.00417 \text{ mA} \times 80 \text{ M}\Omega) = -23.17 \text{ kV}, \quad \text{(A.4)}$$

where I is the current and R_{eq} is the equivalent resistor representing the two filter pots. The electric field is then calculated to be

$$E_{\text{field}} = \frac{V_{BC} - V_{\text{shield}}}{\Delta x} = 486.54 \text{ V/cm}. \quad \text{(A.5)}$$

E field using cathode-anode piercing tracks

We devise an independent method to measure the drift time (and consequently drift velocity and electric field) using TPC cathode to anode piercing tracks. We use this method as a cross check to the single line method. The basic idea is simple:

0. Select cosmic ray events with only 1 reconstructed track
1. Reduce the events to the one containing tracks that cross both anode and cathode
2. Identify the first and last hit of the track
3. Measure the time difference between these two hits (Δt).

This method works under the assumptions that the time it takes for a cosmic particle to cross the chamber ($\sim$ns) is small compared to the charge drift time ($\sim$ hundreds of μs).

We choose cosmic events to allow for a high number of anode to cathode piercing tracks (ACP tracks), rejecting beam events where the particles travel almost perpendicularly to drift direction. We select events with only one reconstructed track to maximize the chance of selecting a single crossing muon (no-michel electron). We utilize ACP tracks because their hits span the full drift length of the TPC, see figure

A.4, allowing us to define where the first and last hit of the tracks are located in space regardless of our assumption of the electric field.

One of the main features of this method is that it doesn't rely on the measurement of the trigger time. Since Δt is the time difference between the first and last hit of a track and we assume the charge started drifting at the same time for both hits, the measurement of the absolute beginning of drift time t_0 is unnecessary. We boost the presence of ACP tracks in the cosmic sample by imposing the following requirements on tracks:

- vertical position (Y) of first and last hits within ± 18 cm from TPC center (avoid Top-Bottom tracks)
- horizontal position (Z) of first and last hits within 2 and 86 cm from TPC front face (avoid through going tracks)
- track length greater than 48 cm (more likely to be crossing)
- angle from the drift direction (phi in figure A.5) smaller than 50 deg (more reliable tracking)
- angle from the beam direction (theta in figure A.5) greater than 50 deg (more reliable tracking)

Tracks passing all these selection requirements are used for the Δt calculation.

For each track passing our selection, we loop through the associated hits to retrieve the timing information. The analysis is performed separately on hits on the collection plane and induction plane, but lead to consistent results. As an example of the time difference, figures A.6 and A.7 represent the difference in time between the last and first hit of the selected tracks for Run-II Positive Polarity sample on the collection and induction plane respectively. We fit with a Gaussian to the peak of the Δt distributions to extract the mean drift time and the uncertainty associated with it.

The long tail at low Δt represents contamination of non-ACP tracks in the track selection. We apply the same procedure to Run-I and Run-II, positive and negative polarity alike.

To convert Δt recorded for the hits on the induction plane to the drift time we employ the formula

$$t_{drift} = \Delta t - t_{S-I} \tag{A.6}$$

where t_{drift} is the time the charge takes to drift in the main volume between the cathode and the shield plane and t_{S-I} is the time it takes for the charge to drift from the shield plane to the induction plane. In Table A.1 we calculated the drift velocity in the S-I region, thus we can calculate t_{S-I} as

$$t_{S-I} = \frac{l_{S-I}}{v_{S-I}} = \frac{4mm}{1.73mm/\mu s} \tag{A.7}$$

where l_{S-I} is the distance between the shield and induction plane and v_{S-I} is the drift velocity in the same region. A completely analogous procedure is followed for the hits on the collection plane, taking into account the time the charge spent in drifting from shield to induction as well as between the induction and collection plane The value for Δt_{drift} , the calculated drift velocity (v_{drift}), and corresponding drift electric field for the various run periods is given in Table A.2 and are consistent with the electric field value calculated with the single line diagram method.

Delta t_{drift}, drift v and E field with ACP tracks

Data Period	Δt_{Drift} [μs]	Drift velocity [mm/μs]	E field [V/cm]
RunI Positive Polarity Induction	311.1 ± 2.4	1.51 ± 0.01	486.6 ± 21
RunI Positive Polarity Collection	310.9 ± 2.6	1.51 ± 0.01	487.2 ± 21
RunII Positive Polarity Induction	315.7 ± 2.8	1.49 ± 0.01	467.9 ± 21
RunII Positive Polarity Collection	315.7 ± 2.7	1.49 ± 0.01	467.9 ± 21
RunII Negative Polarity Induction	315.9 ± 2.6	1.49 ± 0.01	467.1 ± 21
RunII Negative Polarity Collection	315.1 ± 2.8	1.49 ± 0.01	470.3 ± 21
Average Values	314.1	1.50 ± 0.01	474.3 ± 21

Table A.2: Δt for the different data samples used for the Anode-Cathode Piercing tracks study.

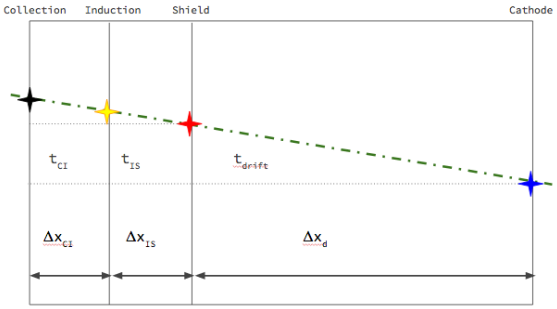

Figure A.4: Pictorial representation of the YX view of the TPC. The distance within the anode planes and between the shield plane and the cathode is purposely out of proportion to illustrate the time difference between hits on collection and induction. An ACP track is shown as an example.

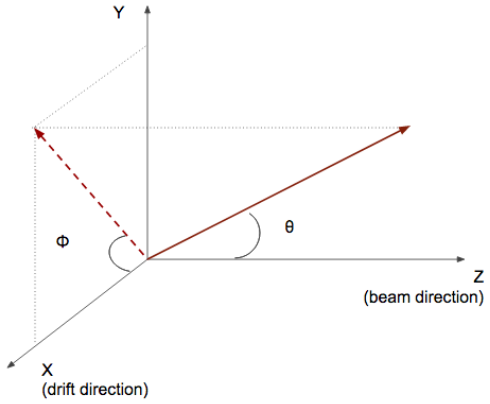

Figure A.5: Angle definition in the context of LArIAT coordinate system.

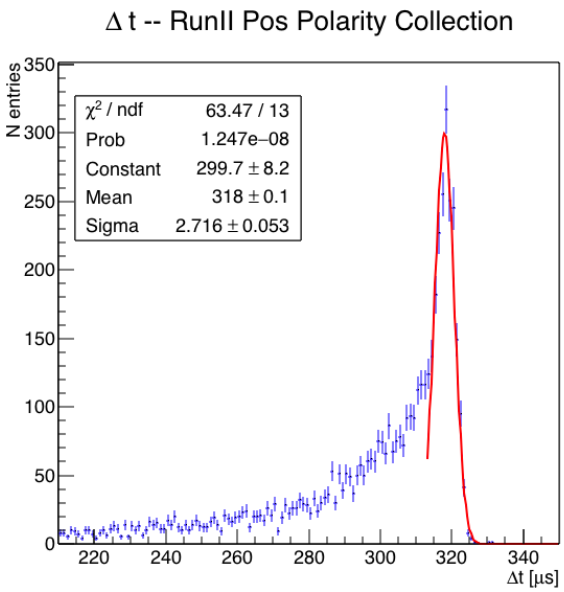

Figure A.6: Collection plane Δt fit for Run II positive polarity ACP data selected tracks.

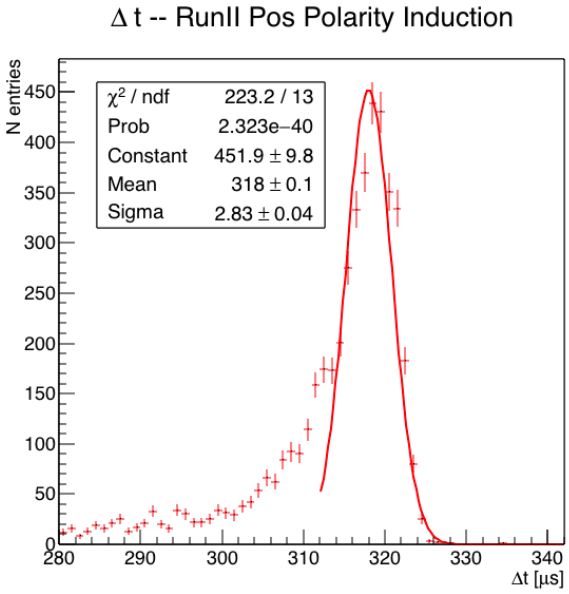

Figure A.7: Induction plane Δt fit for Run II positive polarity ACP data selected tracks.